Geochemistry, petrography and rock magnetism of the basalts of Phek district, Nagaland

Watitemsu Imchen[1], S. K. Patil[2], V. Rino[3], Glenn T. Thong[3,*], Temjenrenla Pongen[3] and B. V. Rao[3]

[1]Geological Survey of India, Northeastern Region, Agartala 799 006, India
[2]Dr K.S. Krishnan Geomagnetic Research Laboratory, Allahabad 221 505, India
[3]Department of Geology, Nagaland University, Kohima Campus, Meriema, Kohima 797 004, India

Basalts occur as sub-alkaline tholeiites in the Naga ophiolite belt. They bear an E-MORB affinity ascribed to aqueous fluid addition from a dehydrating oceanic crust in a supra-subduction zone during the Indo-Burma plate collision. They are commonly altered to spilite. They exhibit relatively poor REE fractionation with almost flat chondrite-normalized patterns. Eu-anomalies are not prominent, indicating the negligible role of plagioclase fractionation in their petrogenesis. Rock magnetic studies suggest that magnetite is the major magnetic mineral in these Upper Cretaceous basalts.

Keywords: Basalt, geochemistry, petrography, rock magnetism.

THE petrogenesis and tectonic setting of the Indian ophiolites occurring in the NW Himalayas and Indo-Myanmar Range (IMR) have attracted much attention[1–6]. The Naga ophiolite belt (NOB) of the IMR is a consequence of collision between the Indian and Burma plates[7]. This NNE–SSW trending arcuate belt extends over 90 km in length and 2–15 km in width[4]. The rocks include peridotite, mafic–ultramafic cumulates, volcanics, meta-basics, oceanic sediments, dykes and minor acid to intermediate intrusives. Basalts form an important component of these ophiolites. Based on petrographic and geochemical attributes, an attempt was made to infer the petrogenesis and tectonic emplacement of the NOB basalt. Rock magnetic studies were attempted to assess the magnetic minerals and their stability.

Geological setting

The NOB represents a remnant of the Tethyan oceanic crust and upper mantle generated at a spreading centre in a narrow, short-lived basin that formed due to rifting and spreading during the Late Cretaceous. The opening and closure of this basin is related to the fragmentation and dispersion of Gondwanaland. The oceanic crust generated was tectonically uplifted together with part of the upper mantle along an active continental margin during the Mid-Eocene[8]. The ophiolites occur between the Disang Group on the west and Nimi Formation in the east where they have been emplaced on the Disang flysch and, in turn, have been overridden by the Nimi Formation.

The study area, including Zipu and its surroundings in Phek district, Nagaland, lies between 25°33′N and 25°41′N and 94°42′E and 94°49′E in topographic maps 83 K/10 and K/14 of the Survey of India (Figure 1)[9]. The Disang Group, comprising a thick sequence of shale intercalated with sandstone, occupies a major portion of the region. Further east, pelagic limestone and radiolarian chert occur in association with mafics and ultramafics. The flysch and mafic–ultramafics are traversed by several easterly dipping thrusts with progressively increasing eastward dips, to almost vertical attitudes, implying their westward tectonic transport[10]. The serpentinized ultramafics comprise harzburgite and dunite. The sporadically occurring mafics, including gabbro, diabase and pyroxenite, do not exhibit any distinct relationship with the ultramafics. The highly dismembered ophiolites form brecciated, fractured and silicified tectonic mix or melange.

After serpentinite, the volcanics are the dominant rocks of the ophiolite suite. Basalts, making up the bulk of the volcanics, occur with minor basaltic andesites, hyaloclastites and pyroclastics, including volcanic breccia, tuff, ash and glass. The volcanics commonly occur along the boundaries of the Disang Group and Nimi Formation. The spilitic basalts of the area probably owe their origin to deuteric alteration of the basaltic flows. The volcanics are mixed with pelagic sediments such as chert and crystalline limestone[3,7,11–13].

Important basalt exposures occur around Thewati, Satuza and Waziho-Zipu, with occasional calcite veins (Figure 1 *a*). To the east of Satuza the volcanics are tectonically sandwiched between serpentinite bodies. To the northeast of Waziho they are intermixed with red chert, without any apparent tectonic dislocation. Rounded to elliptical pillow basalts (Figure 1 *b*), characteristic of

*For correspondence. (e-mail: glen2t03@yahoo.com)

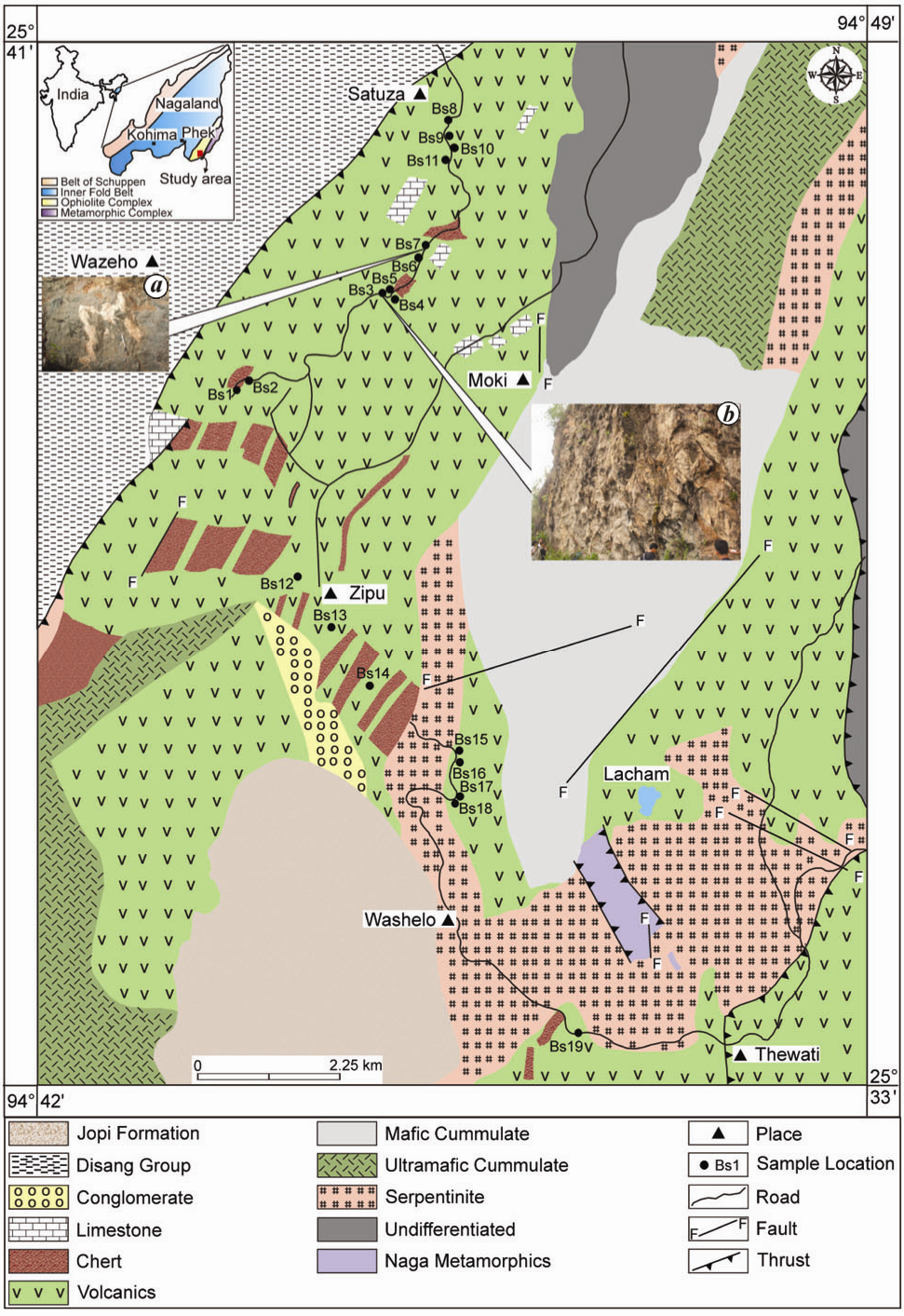

Figure 1. Geological map of the study area (after GSI[9]). (Inset) ***a***, Calcite vein in basalt; ***b***, pillow basalt.

their eruptive nature under submarine conditions, are also noted. The flow tops are bulbous with fractured surfaces and outer glassy chilled margins of variable thicknesses of up to 1.3 cm. This is followed inwards by highly vesicular and central massive, poorly vesicular zones.

The other type of mafic volcanic noted is the sheet flow. The sheet flows exposed between Wazeho and Zipu vary in thickness from 3 to 6 m. These aphanitic basalts, with rounded and elliptical amygdales that are 3–10 mm in diameter, are filled with chalcedony, zeolite, calcite, epidote with secondary quartz, albite and chlorite. No regular lateral or vertical variation in vesicle size is observed. The rims of the vesicles, slightly deformed between Zipu and Moki and oriented along the flow direction, are

occasionally corroded due to reaction with secondary minerals. Chlorite forms rims around the walls of the amygdules, which have cores of calcite. At places the amygdaloidal basalts retain their original texture, but are mostly metamorphosed.

Methods of study

Nineteen representative basalt samples were analysed for the major oxides by XRF method and 19 and 5 samples for the trace and rare earth elements (REE) respectively, by ICP-MS. The REE were normalized against N-MORB[14]. Mg numbers were calculated as follows[15]: Mg# = 100 × MgO/FeO + MgO.

Core (2.2 × 2.5 cm) samples for rock magnetic studies were obtained by standard techniques[16]. Magnetic susceptibility (χlf) and natural remanent magnetization (NRM) for 75 specimens from 19 samples were measured using a MS2B magnetic susceptibility meter and JR-5 spinner magnetometer respectively. The samples were subjected to thermal (TD) and alternating field demagnetization (AFD) methods to identify primary and secondary magnetizations. Characteristic remanent magnetization (ChRM) was determined by principal component analysis[17]. Pulse magnetizer and Molspin magnetometer were used for isothermal remanent magnetization (IRM) studies. Temperature-dependent magnetic susceptibility (kT) experiment was carried out using a KLY-2 Kappabridge (Agico, Czech Republic).

Results

Petrography

The minerals include plagioclase, clinopyroxene and olivine, and their alteration products such as chlorite, epidote, calcite, serpentine and iron oxides. Porphyritic texture is more common than intersertal, spherulitic and variolitic. Spherulite shows radiating aggregates of acicular plagioclase, while variolitic textures are fan-like plagioclase needles within glassy groundmass. Plagioclase, often albitized, occurs as euhedral to subhedral phenocrysts of variable sizes and small acicular microlites, the former being more altered. Lamellar twinned plagioclase crystals showing undulose extinction are commonly altered and clouded (Figure 2). The clouding is due to dark, minute dust-like specks throughout the feldspar crystals. Clinopyroxene phenocrysts are commonly chloritized. Green chlorite occurs along fractures and crystal rims. Anhedral olivine phenocrysts have corroded borders. Incipient alteration to serpentine is noticed. Iron oxides, occurring in the groundmass and along fractures, are late magmatic minerals. Some late felsic veins of quartz cut across the basaltic flows.

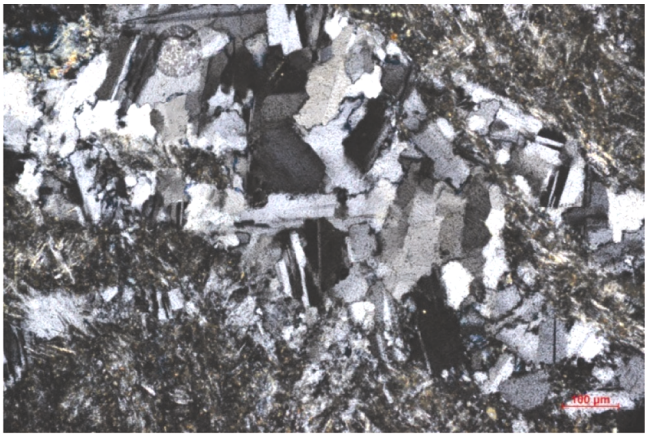

Figure 2. Plagioclase feldspar showing undulose extinction and lamellar twinning.

Rock magnetism

Relatively lower mean χlf and NRM intensity values of 70.38×10^{-5} SI and 6.45×10^{-3} A/m respectively, were noted. However, samples from two sites SE of Wazeho have yielded relatively higher χlf (av. 180×10^{-5} and 690×10^{-5} SI units) and NRM intensities (av. 2.1×10^{-2} and 5.6×10^{-2} A/m). Magnetization saturation took place at 300 mT (Figure 3 *a*), indicating that magnetite is the major magnetic mineral in these samples. Magnetic susceptibility versus temperature (*k*–*T*) curves further corroborate the presence of magnetite as susceptibility drops around 585°C (Figure 3 *b*, 1). The increase in susceptibility with temperature till 550°C for some other samples (Figure 3 *b*, 2) may be ascribed to low-grade metamorphism. However, susceptibility suddenly drops after 580°C, indicating the presence of magnetite.

Major elements

Fe_2O_3/MgO ratios in these basalts are lower than <1.7; most abyssal tholeiites show such low ratios[18]. The NOB is characterized by intermediate to low Ti basalts (<2% TiO_2; Table 1). The negative correlation of TiO_2 and P_2O_5 with MgO ($r = -0.05$ and $r = -0.09$ respectively) indicates enrichment of both oxides with decreasing MgO contents. Both Mg-rich (>10% MgO) and Mg-poor (<10% MgO) basalts are noted. MgO values vary from 4.45 to 14.79 (av. 10.96%), resulting in an Mg# ranging from 33.18 to 66.12 (av. 54.00). The average Na_2O and K_2O of the NOB basalts are 3.65% and 0.54% respectively. The total $Na_2O + K_2O$ values are consistent in all the samples (av. 4.20%). The average Na_2O/K_2O ratio is 9.80, reflecting their sodic affinity. The mobile elements show variable ranges of concentration, suggesting modification of the original composition.

The NOB volcanics are predominantly basaltic with affinity to subalkaline magmas (Figure 4 *a*)[19]. AFM

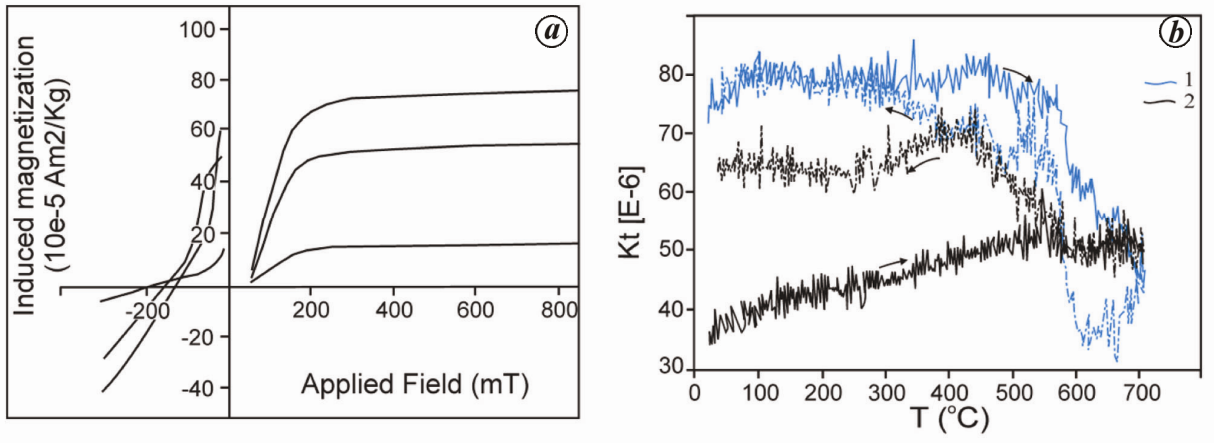

Figure 3. *a*, IRM acquisition curves of representative samples. *b*, 1, 2, Magnetic susceptibility versus temperature curves.

Table 1. Major oxides (%) of NOB basalt

Sample no.	SiO_2	TiO_2	Al_2O_3	Fe_2O_3	MnO	MgO	CaO	Na_2O	K_2O	P_2O_5
Bs1	50.56	0.87	10.76	9.12	0.17	14.79	9.15	3.54	0.89	0.09
Bs2	48.30	1.41	12.10	11.30	0.15	10.80	11.80	2.11	0.76	0.13
Bs3	49.14	1.30	13.88	12.78	0.17	7.12	10.27	3.43	1.12	0.10
Bs4	47.81	1.42	13.69	11.12	0.15	10.31	11.14	2.16	0.34	0.12
Bs5	47.25	1.44	14.04	12.28	0.18	11.46	8.81	3.76	0.50	0.14
Bs6	51.87	0.78	12.16	10.62	0.16	10.15	8.72	3.87	0.27	0.21
Bs7	50.50	1.32	12.11	11.57	0.14	5.90	7.78	3.29	1.25	0.17
Bs8	48.35	1.57	13.52	12.33	0.17	12.22	6.36	4.11	0.25	0.19
Bs9	47.23	1.31	14.32	12.22	0.18	13.04	7.37	3.25	0.55	0.10
Bs10	49.62	1.21	12.81	10.21	0.18	9.14	10.56	3.16	0.67	0.05
Bs11	48.84	1.45	11.48	9.87	0.19	13.59	9.45	4.12	0.31	0.09
Bs12	46.27	1.32	14.42	11.72	0.15	4.45	14.32	3.47	0.19	0.10
Bs13	50.48	0.74	9.98	8.65	0.15	12.92	8.97	4.01	0.14	0.18
Bs14	49.26	1.21	13.25	11.86	0.17	14.53	4.54	4.65	0.32	0.10
Bs15	50.65	1.10	11.67	9.95	0.15	10.48	10.32	3.47	0.87	0.19
Bs16	51.76	1.46	12.78	11.16	0.16	9.21	7.74	4.42	0.61	0.09
Bs17	48.27	1.65	12.42	11.42	0.18	14.32	6.57	3.12	0.28	0.10
Bs18	49.93	1.36	11.57	11.29	0.14	11.52	8.72	4.65	0.35	0.12
Bs19	48.33	1.45	13.13	12.21	0.15	12.49	6.29	4.87	0.58	0.07

($Na_2O + K_2O - Fe_2O_3 - MgO$) plots in the diagram of Irvine and Baragar[20] (Figure 4 *b*), point to a tholeiitic nature.

The negative correlation of SiO_2 with Al_2O_3 ($r = -0.7$), Fe_2O_3 ($r = -0.52$), CaO ($r = -0.23$), MgO ($r = -0.03$) and TiO_2 ($r = -0.56$) is probably due to fractional crystallization of the ferromagnesian minerals such as olivine and clinopyroxene during magmatic evolution. The negative correlation between MgO and CaO ($r = -0.59$) is suggestive of depletion of Mg in clinopyroxene, with stability of Ca content. The inverse correlation of P_2O_5 and MgO ($r = -0.09$) is related to the presence of apatite, which crystallized at a late stage of magma differentiation.

Trace elements

Zr, being relatively immobile, is correlated with some trace elements to determine their degree of remobilization and fractionation. TiO_2, CaO and K_2O increase with increasing Zr while Na_2O, MgO and P_2O_5 show a decrease, suggesting primary fractionation of plagioclase and pyroxene during magma evolution. This is further corroborated by low SiO_2, high MgO (>7%) for most samples and >11% ∑FeO, which are distinctive criteria for the slightly fractionated NOB basalt. The positive correlation of compatible elements such as Ni, Cr and Co with MgO/FeO ratios ($r = 0.06$, 0.76 and 0.30 respectively) may be related to fractional crystallization of olivine and clinopyroxene. The few samples falling in the alkaline field (Figure 4 *b*) indicate sea-water alteration, as these samples have unusually high Na_2O content.

The REE and corresponding trace elements of the five samples analysed were normalized to the primitive mantle composition[14] to know the degree of evolution relative to the mantle (Figure 5 *a*). Plots show variable and selective incompatible-element enrichment, particularly of the large-ion lithophile elements (LILE). These basalts also

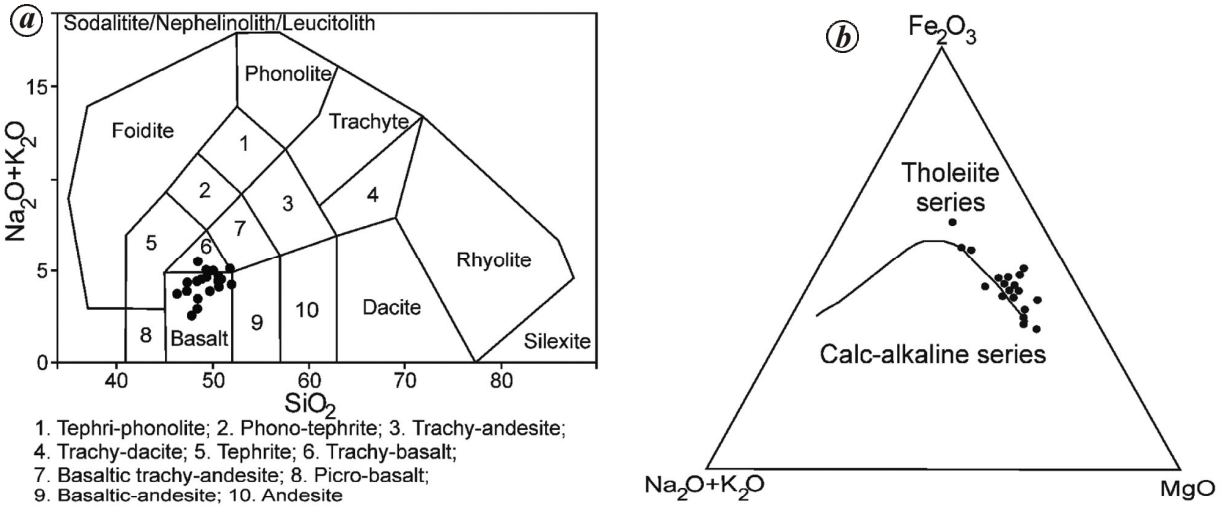

Figure 4. ***a***, Total alkali–silica classification of NOB basalt (after Middlemost[19]). ***b***, AFM plots of NOB basalt (after Irvine and Baragar[20]).

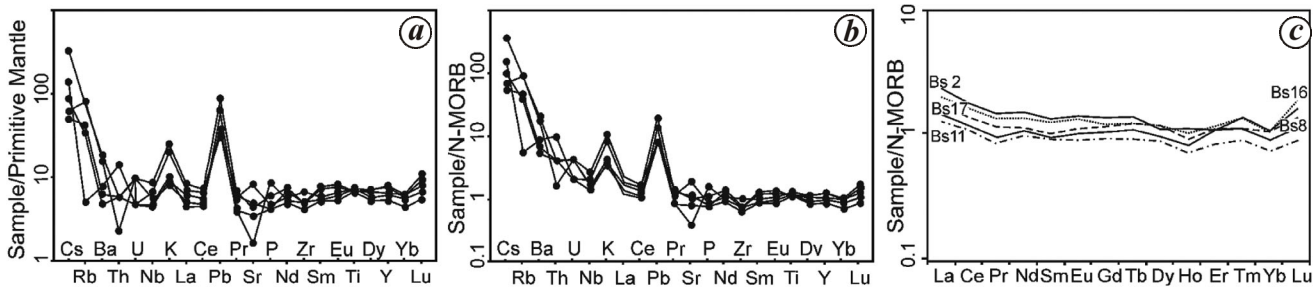

Figure 5. ***a***, Primitive mantle-normalized spidegram of NOB basalt. ***b***, N-MORB-normalized spidergram of NOB basalt. ***c***, N-MORB-normalized REE diagram of NOB basalt (***a***–***c***, after Sun and McDonough[14]).

show high concentrations of Cs, Rb, Ba and Sr (Table 2). A distinctive spiked pattern for K and Pb and pronounced trough at Th, Nb, La and Ce are noted. The same samples normalized to N-MORB[14] show enrichment of LILE relative to the high-field-strength elements (HFSE) (Figure 5 *b*). The REE and HFSE display coherent and subparallel patterns. Most samples show enrichment of Ba, Th, Nb, Sr and Zr relative to N-MORB, suggesting derivation of the parental melt of these basalts from an enriched mantle source similar to an E-MORB, or a source which has experienced some degree of melting. Ti and V behave like pseudo-incompatible elements, their contents increasing with greater fractional crystallization. Similarly, Sr is higher in slightly evolved volcanic magmas. Sr varies from 23 to 495 (av. 126.3 ppm), which is relatively higher than N-MORB (90 ppm). The negative Sr peak may be attributed to removal of Sr with Ca during ocean-floor weathering. The spider diagram shows enrichment of most trace elements, suggesting probable alteration by secondary processes. The scattering of data in most of the bivariate plots may be attributed to hydrothermal metamorphism.

Rare earth elements

The total REE content varies from 36.1 to 54.9, with an average of 45.5 ppm (Table 3). The fractionation ratio of LREE/HREE ranges from 1.07 to 1.84 (av. 1.52). Chondrite-normalized $(La/Yb)_N$ ratios vary from 1.07 to 2.32 (av. 1.70), $(La/Sm)_N$ from 0.83 to 3.16 (av. 1.76), $(Gd/Yb)_N$ from 0.85 to 1.36 (av. 1.10), $(La/Ce)_N$ from 0.63 to 2.64 (av. 1.23), and $(Ce/Yb)_N$ from 0.83 to 2.07 (av. 1.47). REE abundances are normalized to N-MORB[14]. Slight LREE enrichment and almost flat middle and heavy REE patterns with limited negative Eu-anomaly are noted (Figure 5 *c*).

Discussion

Petrogenesis

The presence of plagioclase phenocrysts points to fractional crystallization[21]. The high contents of clinopyroxene and olivine phenocrysts in the basalt may be due to higher MgO content. Variolitic and spherulitic textures

Table 2. Trace elements (ppm) of NOB basalt

Sample no.	Sc	V	Cr	Co	Ni	Cu	Zn	Rb	Sr	Y	Zr	Nb	Cs	Ba	Hf	Ta	Pb	Th	U
Bs1	41	156	303	88	43	131	101	10.30	333	16.2	62.8	3.5	0.1	33	1.5	1.1	4.4	0.1	0.2
Bs2	45	275	218	72	120	78	156	53.40	91	29.9	56.2	6.2	2.6	112	1.9	2.1	5.9	0.2	0.2
Bs3	35	321	172	68	76	123	109	9.50	156	35.4	64.1	6.6	0.1	160	1.8	0.9	3.2	0.1	0.2
Bs4	33	325	198	51	66	58	113	15.30	495	37.2	62.5	4.1	1.5	126	1.9	1.8	3.4	1.2	0.1
Bs5	33	345	249	70	46	88	127	21.20	87	23.6	39.7	1.6	0.6	128	1.5	0.7	2.7	0.3	0.1
Bs6	33	221	212	46	54	111	113	8.50	260	18.1	43.8	5.8	0.3	20	0.8	2.3	2.7	0.3	0.2
Bs7	34	237	127	56	62	72	104	24.60	93	24.8	37.2	3.3	0.1	41	0.8	0.9	4.2	0.2	0.2
Bs8	33	265	221	65	77	83	120	22.00	35	27.6	55.3	4.0	0.7	34	2.1	0.8	4.2	0.5	0.2
Bs9	37	255	254	93	63	141	115	8.60	23	19.7	52.7	7.3	2.1	18	1.2	2.6	2.6	0.4	0.1
Bs10	41	247	175	90	118	38	111	13.20	71	37.6	72.3	5.5	0.5	83	1.8	0.9	2.9	0.4	0.1
Bs11	37	234	182	76	123	99	131	3.20	72	24.4	46.7	3.3	1.1	55	1.5	1.1	2.6	1.2	0.1
Bs12	44	312	85	68	88	71	174	22.10	57	19.5	39.5	3.7	0.5	50	1.6	1.2	2.5	0.2	0.1
Bs13	46	347	243	60	110	99	160	16.80	92	34.7	69.4	1.2	1.2	20	1.6	2.4	3.8	0.1	0.1
Bs14	44	324	272	62	47	86	178	3.20	121	29.9	38.8	13.6	1.1	147	2.1	1.1	3.5	0.2	0.1
Bs15	41	272	258	72	72	83	132	1.50	40	34.2	41.2	3.5	0.4	17	1.1	2.6	2.4	1.2	0.2
Bs16	42	198	112	66	33	51	125	26.80	102	35.7	55.2	4.8	0.4	44	1.6	1.4	2.4	0.5	0.1
Bs17	35	382	212	78	78	76	121	50.30	175	35.5	75.1	3.2	0.5	133	1.8	2.4	2.6	0.5	0.1
Bs18	35	235	219	68	140	91	130	12.40	49	32.8	42.6	6.2	1.1	44	1.2	2.8	2.5	0.5	0.2
Bs19	47	272	234	94	47	122	151	25.30	48	25.3	45.3	13.9	0.5	19	2.2	1.2	2.5	0.3	0.3

Table 3. Rare earth elements (ppm) of NOB basalt

Sample	Bs2	Bs8	Bs11	Bs16	Bs17
La	5.70	3.50	3.10	4.80	4.20
Ce	12.90	8.50	8.00	11.80	9.90
Pr	1.90	1.20	1.10	1.70	1.50
Nd	10.30	7.30	6.80	9.40	7.90
Sm	3.40	2.40	2.30	3.20	2.60
Eu	1.40	1.00	0.90	1.30	1.10
Gd	4.90	3.70	3.30	4.30	4.20
Tb	0.90	0.70	0.60	0.80	0.80
Dy	4.90	4.20	3.90	5.20	5.20
Ho	1.10	0.80	0.70	1.00	0.90
Er	3.10	3.10	2.40	3.30	3.20
Tm	0.60	0.50	0.40	0.60	0.50
Yb	3.10	2.70	2.20	2.90	3.10
Lu	0.70	0.50	0.40	0.80	0.60
∑REE	54.90	40.10	36.10	51.10	45.70
Eu/Eu*	1.04	1.02	0.99	1.06	1.01
LREE/HREE	1.65	1.33	1.44	1.53	1.33
$(La/Yb)_N$	2.24	1.58	1.72	2.02	1.65
$(La/Sm)_N$	1.76	1.53	1.42	1.58	1.70
$(Gd/Yb)_N$	1.31	1.14	1.24	1.23	1.12
$(La/Ce)_N$	1.32	1.23	1.16	1.22	1.27
$(Ce/Yb)_N$	1.69	1.28	1.47	1.65	1.29

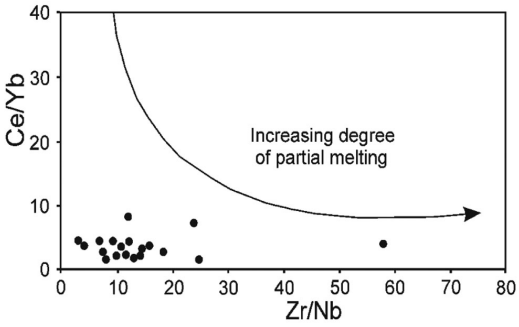

Figure 6. Binary plots of Ce/Yb versus Zr/Nb of NOB basalt (after Bagci[24]).

are ascribed to devitrification of glass[22]. The tholeiitic trend suggests that oxygen fugacity of the magma chamber was low, as high oxygen fugacity produces calc-alkaline trends[23].

High Mg# indicates a primitive mantle source[15]. Intermediate Mg# of the NOB basalts (33.18–66.12; av 54) suggests a slightly evolved magmatic source. This is corroborated by the slightly higher contents of Cr and Ni. In the Ce/Yb versus Zr/Nb diagram (Figure 6) of Bagci[24], a few samples suggest higher degrees of partial melting of the mantle. This implies that the influence of partial melting in the petrogenesis of the NOB tholeiitic basalt cannot be ruled out.

Melting experiments suggest that high-alumina basaltic liquids are not products of low pressure fractionation[25]. The lower content of Al_2O_3 (9.90–14.40; av. 12.60) of the NOB basalts relative to the N-MORB (15.27) suggests fractionation at relatively lower pressures, implying that these basalts were emplaced from a shallower magma source.

The Zr/Nb ratios of the NOB tholeiites range from 3.25 to 24.80 (av. 11.90), with an exception of sample Bs13 (57.00), which are relatively lower than the N-MORB (>30), suggesting enrichment in the mantle. The $(La/Sm)_N$ ratio, an index of mantle enrichment, is slightly higher in the NOB basalts (1.07–2.32; av. 1.79), which also suggests an enriched mantle source. This is further corroborated by higher ratios of Ta/Nb (0.08–2.00; av. 0.42) compared to 0.06 of most N-MORB[14].

Primitive mantle-normalized spidergrams show variable and selective incompatible element enrichment. Primitive mantle- and N-MORB-normalized spidergrams

of the NOB basalts are characterized by enrichment of LILE such as Rb, Ba, Cs and K relative to REE and HFSE. As these elements are mobile, they could have been enriched by remobilization during seafloor alteration or metamorphism related to collision or obduction. Their enrichment also suggests that these rocks were selectively metasomatized in a supra-subduction zone (SSZ)[26].

Nb and Ta are enriched relative to N-MORB in the NOB basalt, except for two samples with negative Nb anomaly. Wood *et al.*[27] have suggested that negative Nb and Ta anomalies are characteristic of rocks of volcanic arcs. Subduction-related mobile elements such as Ba and Pb are enriched relative to REE. The overall flat REE pattern with limited negative Eu anomaly suggests that the parent magma was poorly fractionated. It implies that Eu^{2+} substitution for Ca^{2+} was limited in the plagioclase feldspar during fractional crystallization[28].

Selective enrichment of Sr, Ba and U and relative lack of Zr, Y and Hf are noted in the spidergrams. Such patterns and HFSE variations exhibited by tholeiitic rocks are characteristic of a SSZ[29]. To evaluate the nature of the sediment component in modulating the composition of the lavas, the mobile nature of Ba and immobility of Th and Nb have been used effectively. Low Th/Nb is considered as derived from low sediment sources. The Th/Nb ratios of the NOB tholeiitic lavas vary from 0.02 to 0.36 (av. 0.10). This average is significantly higher than the N-MORB composition (0.05), suggesting contamination by the subducting slab. Low Zr/Nb ratios (3.25–24.8) imply chemical modification due to addition from a subducting component[30]. High La/Ti and enriched LILE, and negative Nb and Ti anomalies in the N-MORB normalized spidergrams are ascribed to crustal contamination, which may be due to dehydration of the subducted slab[31,32].

Geochemical data of the NOB basalts resemble those of E-MORB. Schilling[33] explained the origin of E-MORB as due to interaction of enriched plumes from the deep mantle with depleted upper mantle sources of N-MORB. According to Donnelly *et al.*[34], the origin of E-MORB far from hot spots is debatable. Other sources of enrichment include fractionation during melting or metasomatic events[35,36]. The origin of the NOB basalts by plume enrichment is rather unlikely; limited negative Eu anomaly suggests poor crystal fractionation. Many workers have suggested that back-arc basin basalts which form by partial fusion of mantle sources are analogous to those involved in the generation of normal or slightly enriched MORB[37,38]. Wilson[39] suggested that major element geochemistry of back-arc basin basalts has similar characteristics with MORB, although they generally seem to have greater affinity with E-MORB composition. However, emplacement of the NOB basalt in a back-arc setting is most unlikely as the back-arc lies beyond the volcanic arc to the east. The NOB basalts are part of a fore-arc setting, as shown by other studies[40]. The enrichment therefore, may be attributed to aqueous fluid addition from a dehydrating subducting oceanic crust such as the Indo-Burma plate collision. This is further substantiated by negative P and Nb anomalies, and peak at Pb. Such anomalies are ascribed to magmatic contamination by continental crust[31,32,41].

Metamorphism/secondary alteration

Hughes[42] proposed the $K_2O + Na_2O$ versus $K_2O/(K_2O + Na_2O) \times 100$ diagram to show alkali metasomatism in igneous rocks. In this diagram most NOB basalts show some alkali metasomatism (Figure 7 *a*), probably to spilite. This is further corroborated by high albite content (17.85–37.40; av. 27.00) in these basalts. Undulose extinction and dissolution of plagioclase (Figure 2) also indicate effects of metamorphism.

The NOB basalts have suffered low-grade metamorphism and hydrothermal alteration[12]. During such activity most ophiolitic basalts suffer elemental migration[43]. Seawater alteration of ocean floor rocks may modify the mobile element (Rb, Sr, K, Ba and U) contents, but it generally does not affect HFSE and REE[44]. The N-MORB normalized plots (Figure 5 *b*) suggest that the NOB basalts underwent variable degrees of hydrothermal and/or incipient metamorphism. Variable concentrations of the mobile elements indicate modification of the original composition, while the subparallel pattern of the HFSE and REE indicates little mobility. The enrichment of most trace elements may be due to alteration by secondary processes. Mineralogical and chemical alteration of volcanic sequences of ophiolites by submarine hydrothermal alteration processes is well documented[45,46]. The scattering of data in the bivariate plots may be attributed to low temperature–high pressure metamorphism, which is evident by the association of greenschist, glaucophane-schist and eclogite facies noted in the NOB with the basalt and chert[47].

Age of the NOB basalts

Sarkar *et al.*[48] reported a single radiometric age of 148 ± 4 Ma (whole rock K–Ar) from a basalt flow found juxtaposed with red and green cherts, southeast of the present sample sites. These basic to intermediate volcanic rocks are intercalated with variegated chert and occasionally with limestone. The presence of silica-secreting organisms such as radiolaria in the bedded chert suggests their accumulation in the abyssal floor below the carbonate compensation depth (CCD). The isolated ChRM direction from two sites (Bs2, Bs4) of ongoing palaeomagnetic studies on these basalts yields a Late Cretaceous age. These two basalt sites are intimately associated with limestone representing the upper part of the oceanic crust, which was probably emplaced above the CCD.

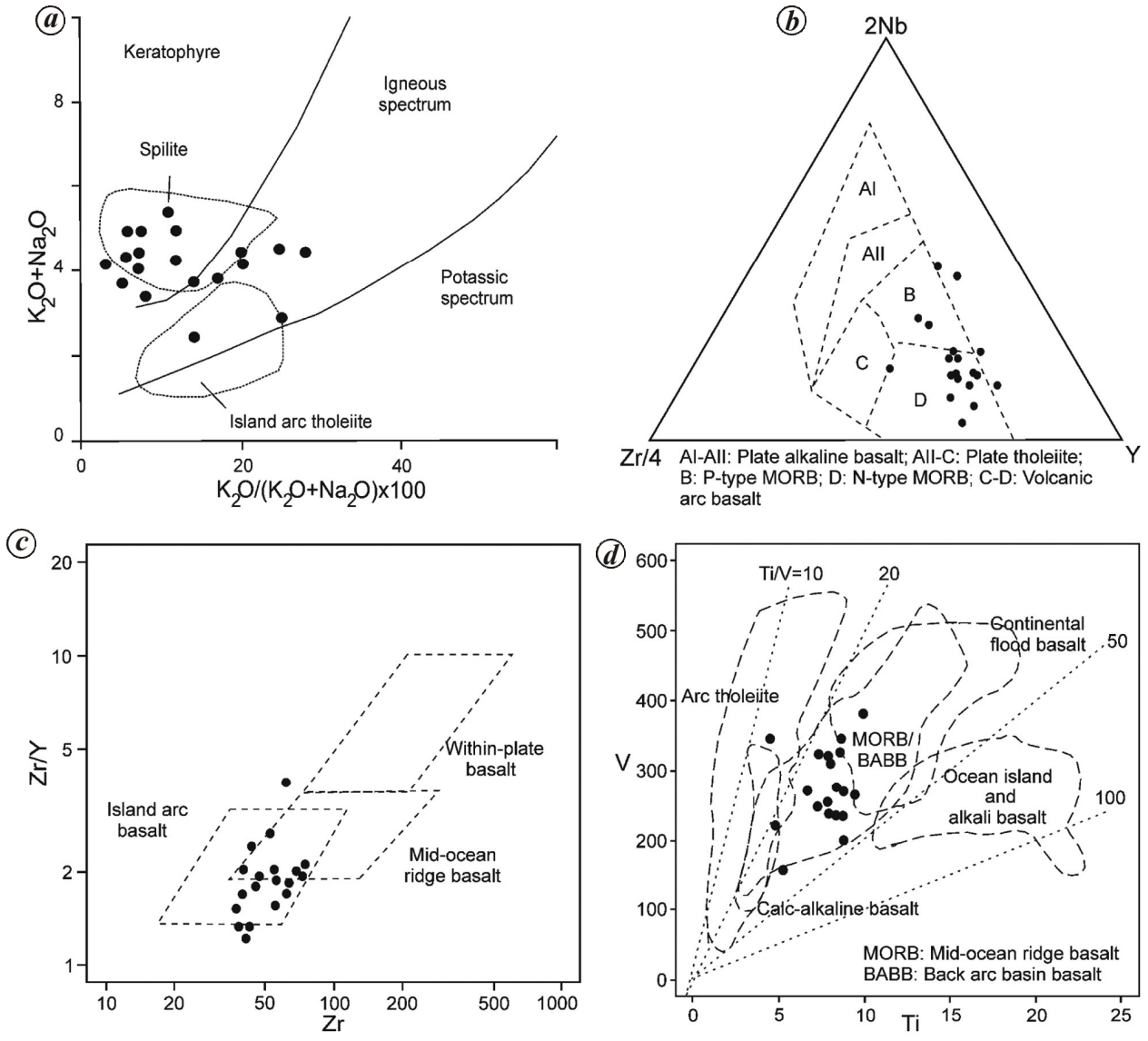

Figure 7. ***a***, K_2O+Na_2O versus $K_2O/(K_2O+Na_2O) \times 100$ plots of NOB basalt (after Hughes[42]). ***b***, Nb–Zr–Y tectonic discrimination plots of NOB basalt (after Meschede[51]). ***c***, Zr versus Zr/Y tectonic discrimination plots of NOB basalt (after Pearce and Norry[52]). ***d***, V versus Ti discrimination diagram of NOB basalt (after Shervais[53]).

Tectonic setting and evolution

Basalts are generated in different oceanic environments such as mid-ocean ridges, back-arc and fore-arc basins, leaky transform faults and immature island arcs[49]. Their evolution in different oceanic environments gives rise to considerable geochemical and petrological complexities due to mantle heterogeneities, magma mixing, contamination and fractional processes. The geochemical characteristics of the NOB basalts are utilized to trace the evolution of their tectonic environment.

Plots in the Nb–Zr–Y tectonic discrimination diagram (Figure 7 *b*)[50] suggest that these basalts were emplaced both as N-MORB and E-MORB. The NOB basalt samples plotted in the Zr versus Zr/Y discrimination diagram (Figure 7 *c*)[51] show both MORB and island arc characteristics. As vanadium and titanium are strongly incompatible and immobile, they are used to discriminate volcanic arc tholeiites, MORB and alkali basalts. In the V/Ti plots (Figure 7 *d*)[52], most samples plot in the fields of MORB and back-arc basin basalts. However, as discussed earlier, they are fore-arc basalts[40]. The overall geochemical signatures indicate ocean floor tholeiite character and have been probably emplaced as MORB. The oceanic crust thus generated was tectonically uplifted along with the upper mantle due to eastward subduction of the Indian plate beneath the Burma plate. By Mid-Eocene a stack of ophiolite slices was created, as evidenced by the ages of the Upper Disang Formation[8] and the ophiolite-derived Phokphur sediments[40].

Conclusion

The low TiO_2 NOB basalts are predominantly tholeiitic and sub-alkaline. These ocean floor tholeiites bear an E-MORB affinity. They originated due to melting of a mantle source that probably underwent limited shallow-level fractionation. The MORB enrichment is due to aqueous fluid addition from a dehydrating subducting oceanic crust in a SSZ during collision of the Indian and Burma plates. Magnetite is the carrier of stable remanent magnetization. Variable degrees of hydrothermal and low-temperature–high-pressure metamorphism of these Late Cretaceous basalts seem to have affected the magnetic stability of most of the NOB basalts.

1. Brunnschweiler, R. O., On the geology of Indo-Burman ranges. *J. Geol. Soc. Austr.*, 1966, **13**, 137–195.
2. Moores, E. M., Origin and emplacement of ophiolites. *Rev. Geophys. Space Phys*., 1982, **20**, 735–760.
3. Agrawal, O. P. and Kacker, R. N., Nagaland ophiolites, India: a subduction zone ophiolite complex in a Tethyan orogenic belt. In *Ophiolites* (ed. Panayiotou, A.), Proceedings of International Ophiolite Symposium, Cyprus, 1980, pp. 454–461.
4. Ghose, N. C., Agrawal, O. P. and Singh, R. N., Geochemistry of the ophiolite belt of Naga Hills, N.E. India. In *Ophiolite and Indian Plate Margin* (eds Ghose, N. C. and Varadaranjan, S.), Sumna Publ., Patna, 1986, pp. 241–293.
5. Sengupta, S., Ray, K. K., Acharyya, S. K. and De Smith, J. B., Nature of ophiolite occurrences along the eastern margin of the Indian plate and their tectonic significance. *Geology*, 1990, **18**, 439–442.
6. Guillot, S., Maheó, G., De Sigoyer, J., Hattori, K. H. and Pêcher, A., Tethyan and Indian subduction viewed from the Himalayan high to ultrahigh-pressure metamorphic rocks. *Tectonophysics*, 2008, **451**, 225–241.
7. Acharyya, S. K., Ray, K. K. and Roy, D. K., Tectono-stratigraphy and emplacement history of the ophiolite assemblage from the Naga Hills and Andaman Island Arc, India. *J. Geol. Soc. India*, 1989, **33**(1), 4–18.
8. Imchen, W., Thong, G. T. and Pongen, T., Provenance, tectonic setting and age of the sediments of the Upper Disang Formation in the Phek District, Nagaland. *J. Asian Earth Sci*., 2014, **88**, 11–27.
9. Geological Survey of India, Geology of Nagaland ophiolite. D.B. Ghosh Commemorative Volume. *Mem. Geol. Surv. India*, 1986, **119**, 1–113.
10. Duarah, R., Saikia, M. M. and Bhattacharjee, C. C., Occurrence of the ophiolite complex along the Indo-Burman orogenic belt. *Geol. Mag*., 1983, **120**, 175–182.
11. Directorate of Geology and Mining, Nagaland. Miscellaneous Publication No. 1, 1978.
12. Venkataramana, P., Datta, A. K. and Acharyya, S. K., Petrography and petrochemistry of the ophiolite suite. *Mem. Geol. Soc. India*, 1986, **119**, 33–63.
13. Ezung, O. C., Petrography and geochemistry of volcanic rocks of the ophiolite suite in and around Zipu, Phek district, Nagaland. Ph D thesis, Nagaland University, Kohima, 2007.
14. Sun, S. S. and McDonough, W. F., Chemical and isotopic systematics of oceanic basalts: implications for mantle composition and processes. In *Magmatism in the Ocean Basins* (eds Saunders, A. D. and Norray, M. J.), *Geol. Soc. London, Spl. Publ.*, 1989, **42**, 313–345.
15. Reichow, M. K., Saunders, A. D. and White, R. V., Geochemistry and petrogenesis of basalts from the west Siberian basin: an extension of the Permo-Triassic Siberian Traps, Russia. *Lithos*, 2005, **79**, 435–452.
16. Butler, R. F., *Paleomagnetism: Magnetic Domains to Geologic Terranes*, Blackwell Science Inc., Oxford, 1998 (electronic edition).
17. Kirschvink, J. L., The least-square line and plane and the analysis of paleomagnetic data. *Geophys. J. Roy. Astron. Soc*., 1980, **62**, 699–718.
18. Miyashiro, A., Volcanic rock series in island arcs and active continental margins. *Am. J. Sci*., 1974, **274**, 321–355.
19. Middlemost, E. A. K., Naming materials in the magma/igneous rock system. *Earth Sci. Rev*., 1994, **37**, 215–224.
20. Irvine, T. N. and Baragar, W. R. A., A guide to the chemical classification of the common volcanic rocks. *Can. J. Earth Sci*., 1971, **8**, 523–548.
21. Roy, A., Bandyopadhyay, B. K. and Huin, A. K., Geology and geochemistry of basic volcanics from the Sakoli schist belt of Central India. *J. Geol. Soc. India*, 1997, **50**, 209–221.
22. Winter, J. D., *An Introduction to Igneous and Metamorphic Petrology*, Prentice Hall, New Jersey, 2001, pp. 30–45.
23. Coleman, D. and Walker, J. D., Geochemistry of Mio-Pliocene volcanic rocks from around Panamint Valley, Death Valley area, California. *Geol. Soc. Am. Mem.*, 1990, **176**, 391–411.
24. Bagci, U., The geochemistry and petrology of the ophiolitic rocks from the Kahramanmaras region, southern Turkey. *Turk. J. Earth Sci.*, 2013, **22,** 1–27.
25. Ringwood, A. E., *Composition and Petrology of the Earth's Mantle*, McGraw Hill Book Company, New York, 1976, p. 618.
26. Tatsumi, Y., Hamilton, D. L. and Nesbitt, R. W., Chemical characteristics of fluid phase released from a subducted lithosphere and origin of arc magmas: evidence from high-pressure experiments and natural rocks. *J. Volcanol. Geotherm. Res*., 1986, **29**, 293–309.
27. Wood, D. A., Joron, J. L. and Treuil, M., A re-appraisal of the use of trace elements to classify and discriminate between magma series erupted in different tectonic settings. *Earth Planet. Sci. Lett*., 1979, **45**, 326–336.
28. Rollinson, H. R., *Using Geochemical Data: Evaluation, Presentation, Interpretation*, John Wiley, New York, 1993, p. 344.
29. Pearce, J. A., Lippard, S. J. and Robert, S., Characteristics and tectonic significance of supra-subduction zone ophiolite. In *Marginal Basin Geology* (eds Kokelaar, B. P. and Howells, M. F.), *Geol. Soc. London, Spl. Publ*., 1984, **16**, 77–94.
30. Ray, D., Rajan, S. and Ravindra, R., Role of subducting component and sub-arc mantle in arc petrogenesis: Andaman volcanic arc. *Curr. Sci*., 2012, **102**, 605–609.
31. Cox, K. G. and Hawkesworth, C. J., Relative contributions of crust and mantle to flood basalt magmatism, Mahabaleshwar area, Deccan Traps. *Philos. Trans. R. Soc. London, Ser. A*, 1984, **310**, 627–641.
32. Wooden, J. L. *et al.*, Isotopic and trace element constraints on mantle and crustal contributions to Siberian continental flood basalts. Noril'sk area, Siberia. *Geochim. Cosmochim. Acta*, 1993, **57**, 3766–3704.
33. Schilling, J. G., Iceland mantle plume: geochemical study of the Reykjanes Ridge. *Nature*, 1973, **242**, 565–571.
34. Donnelly, K. E., Goldstein, S. L. and Langmuir, C. H., Origin of enriched ocean ridge basalts and implications for mantle dynamics. *Earth Planet. Sci. Lett*., 2004, **226**, 347–366.
35. Halliday, A. N., Lee, D. C., Tommasini, S., Davies, G. R., Paslick, C. R., Fitton, J. G. and James, D. E., Incompatible trace elements in OIB and MORB and source enrichments in the sub-oceanic mantle. *Earth Planet. Sci. Lett*., 1995, **133**, 379–395.
36. McKenzie, D. P. and O'Nions, R. K., The source regions of ocean island basalts. *J. Petrol*., 1995, **36**, 133–159.
37. Hawkesworth, C. J., O'Nions, R. K., Pankhurst, R. J., Hamilton, P. J. and Evensen, N. M., A geochemical study of island arc and

back arc tholeiites from the Scotia Sea. *Earth Planet. Sci. Lett*., 1977, **36**, 253–262.
38. Saunder, A. D. and Tarney, J., The geochemistry of basalts from a back arc spreading centre in the East Scotia Sea. *Geochim. Cosmochim. Acta*, 1979, **43**, 555–572.
39. Wilson, M., *Igneous Petrogenesis: A Global Tectonic Approach*, Harper Collins Academic Publishers, London, 1989, p. 240.
40. Acharyya, S. K., Collisional emplacement history of the Naga–Andaman ophiolites and the position of the eastern Indian suture. *J. Asian Earth Sci*., 2007, **29**, 229–242.
41. Peng, Z. X., Mahoney, J. J., Hooper, P. R., Harris, C. and Beane, J. E., A role for lower continental crust in flood basalt genesis: isotopic and incompatible element study of the lower six formations of the western Deccan Traps, India. *Geochim. Cosmochim. Acta*, 1994, **58**, 267–288.
42. Hughes, J. C., Spilites, kerotophyres and the igneous spectrum. *Geol. Mag*., 1972, **109**, 513–527.
43. Hart, R. A., Chemical exchange between sea water and deep ocean basalts. *Earth Planet. Sci. Lett*., 1970, **9**, 269–279.
44. Verma, S. P., Seawater alteration effects on REE, K, Rb, Cs, Sr, U, Th, Pb and Sr–Nd–Pb isotope systematics of mid-ocean ridge basalt. *Geochem. J*., 1992, **26**, 159–177.
45. Pearce, J. A. and Cann, J. R., Tectonic setting of basic volcanic rocks determined by using trace element analysis. *Earth Planet Sci. Lett*., 1973, **19**, 290-300.
46. Spooner, E. T. and Fyfe, W. S., Sub-seafloor metamorphism, heat and mass transfer. *Contrib. Mineral. Petrol*., 1973, **42**, 287–304.
47. Ghose, N. C., Agrawal, O. P. and Chatterjee, N., Geological and mineralogical study of eclogite and glaucophane schists in the Naga Hills Ophiolite, Northeast India. *Island Arc*, 2010, **19**, 336–356.
48. Sarkar, A., Datta, A. K., Poddar, B. C., Bhattacharyya, B. K., Kollapuri, V. K. and Sanwal, R., Geochronological studies of Mesozoic igneous rocks from eastern India. *J. SE Asian Earth Sci*., 1996, **13**, 77–81.
49. Shervais, J. W., Birth, death and resurrection: the life cycle of supra-subduction zone ophiolites. *Geochem. Geophys. Geosyst*., 2001, **2**, paper no. 2000GC000080.
50. Meschede, M., A method of discriminating between different types of mid-ocean ridge basalts and continental tholeiites with the Nb–Zr–Y diagram. *Chem. Geol*., 1986, **56**, 207–218.
51. Pearce, J. A. and Norry, M. J., Petrogenetic implications of Ti, Zr, Y, and Nb variations in volcanic rocks. *Contrib. Mineral. Petrol*., 1979, **69**, 33–47.
52. Shervais, J. W., Ti–V plots and petrogenesis of modern ophiolitic lavas. *Earth Planet. Sci. Lett*., 1982, **59**, 101–118.

ACKNOWLEDGEMENTS. We thank DST, New Delhi for the project ESS/16/249(4)/2005, 15.12.2006. We also thank Dr Temsulemba Walling (Department of Geology, Nagaland University) and Dr Merangsoba (ONGC, Bokaro) for help during fieldwork and the anonymous reviewers for constructive comments that helped improve the manuscript.

Received 2 April 2014; revised accepted 23 April 2015